Journal of Sound and Vibration 329 (2010) 3137–3148

Contents lists available at ScienceDirect

Journal of Sound and Vibration

journal homepage: www.elsevier.com/locate/jsvi

Experimental bifurcations and chaos in a modified self-sustained macro electromechanical system

C.A. Kitio Kwuimy [a,b,*], B. Nana [a], P. Woafo [a]

[a] Laboratory of Modelling and Simulation in Engineering and Biological Physics, University of Yaounde I, Box 812, Yaounde, Cameroon
[b] African Institute for Mathematical Sciences (AIMS), 6 Melrose Road, Muizenberg 7945, South Africa

ARTICLE INFO

Article history:
Received 15 June 2009
Received in revised form
26 November 2009
Accepted 2 February 2010
Handling Editor: L.N. Virgin
Available online 15 March 2010

ABSTRACT

A class of self-sustained Macro ElectroMechanical (MaEMS) Systems is made up of a Rayleigh–Duffing oscillator actuating a mechanical arm through a magnetic coupling. In this paper, to avoid experimental constraints, an audio amplifier is added to the device. Quenching phenomenon, bifurcation and chaos are predicted and shown to occur in a device of this class of MaEMS. Especially by using linear stability analysis, the condition for the quenching phenomenon is derived. Chaos and bifurcation are predicted using Lyapunov exponent and bifurcation diagram. A prototype of device is designed and fabricated. Experimental results for this device that are consistent with results from theoretical investigations are presented and convincingly show quenching phenomenon, bifurcation and chaos.

1. Introduction

ElectroMechanical Systems (EMS) are made of two main parts (electrical and mechanical) coupled together via magnetic, piezoresistive, piezoelectric and capacitive couplings [1–13]. Depending on their dimensions, they are called nano (dimension less than one cubic micrometer), micro (dimension less than one cubic millimeter), and Macro-ElectroMechanical Systems, denoted as NEMS, MEMS and MaEMS respectively. If MEMS and NEMS are now more attractive worldwide, MaEMS still have interest since they are present in various engineering and domestic equipments. Moreover, their modeling equations, which are not more different than those of MEMS and NEMS, present some complexities which are interesting and stimulating challenges, both mathematically and numerically. A large class of magnetically actuated MaEMS are modeled by a set of coupled nonlinear differential equations which sometime involve a time delay [5–10]. MaEMS can be ideal, when the excitation is not influenced by the response of the vibrating system, and nonideal MaEMS in the other case. See Refs. [11,12] for some examples of nonideal MaEMS. Our attention, in this paper is focussed on ideal magnetically actuated MaEMS with a flexible arm and we assume an ideal transfer of energy between the parts of the system. They can be integrated in wide range of applications such as pharmaceutical and cosmetic industries.

Electromechanical systems can be divided into two main classes named autonomous and non-autonomous systems. Non-autonomous electromechanical systems need external excitation to run. Many of them are described by equations of

* Corresponding author at: African Institute for Mathematical Sciences (AIMS), 6 Melrose Road, Muizenberg 7945, South Africa. Tel.: +27733145908.
E-mail address: kwuimy@yahoo.fr (C.A. Kitio Kwuimy).
URL: http://users.aims.ac.za/~cedrick/ (C.A. Kitio Kwuimy).

0022-460X/$ - see front matter © 2010 Elsevier Ltd. All rights reserved.
doi:10.1016/j.jsv.2010.02.003

the general form

$$\frac{d^2y}{dt^2}+\varepsilon_1\frac{dy}{dt}+\mathbf{F}(y)=\mathbf{H}\left(x,\frac{\partial x}{\partial t}\right)+E_0\sin\Omega t, \tag{1}$$

$$\frac{\partial^2x}{\partial t^2}+\varepsilon_2\frac{\partial x}{\partial t}+\mathbf{f}(x,z)=\mathbf{h}\left(y,\frac{dy}{dt}\right), \tag{2}$$

where the mechanical displacement $x(z,t)$ is taken as a function of time t and position z along the flexible arm and $\mathbf{F}(y)$ and $\mathbf{f}(x,z)$ are functions depending on system properties. $\mathbf{H}(x,dx/dt)$, $\mathbf{h}(x,dx/dt)$ are related to the coupling; their nature depends on the type of coupling. These functions show how the electric signal is converted into mechanical motion and vice versa. Many nonlinear phenomena are known from such systems: multiperiodic motion, bifurcation, chaos, parametric and sub or super resonances which could have undeniable applications in engineering (see Refs. [5–13] and references therein for more details).

Another important class of electromechanical systems are self-sustained with one component being of the type Van der Pol or Rayleigh oscillators. The particular interest in this class of EMS is certainly related to the fact that no external excitation is needed. One large class of autonomous electromechanical devices is described by the following type of equations

$$\frac{d^2y}{dt^2}-\varepsilon_1\left(1-g\left(y,\frac{dy}{dt}\right)\right)\frac{dy}{dt}+\mathbf{F}(y)=\mathbf{H}\left(x,\frac{\partial x}{\partial t}\right), \tag{3}$$

$$\frac{\partial^2x}{\partial t^2}+\varepsilon_2\frac{\partial x}{\partial t}+\mathbf{f}(x,z)=\mathbf{h}\left(y,\frac{dy}{dt}\right). \tag{4}$$

These equations are those of systems where self-sustained oscillations are of electric origin (the case considered in this work) and its nature depends on the form of the dissipative function $\mathbf{g}(y,dy/dt)$. If $\mathbf{g}(y,dy/dt)$ contained only odd power of the dynamics variable y, that is $\mathbf{g}(y,dy/dt)=\sum_{n=1}^{N}\alpha_{2n}y^{2n}$, the system would be driven by a Van der Pol oscillator. But if $\mathbf{g}(y,dy/dt)=\sum_{n=1}^{N}\alpha_{2n}(dy/dt)^{2n}$, it would be a Rayleigh oscillator. The system will present Duffing nonlinearity if $\mathbf{F}(x)$ and/or $\mathbf{f}(x,z)$ can take the form $\mathbf{F}(x)=\sum_{n=0}^{N}\alpha_{2n+1}x^{2n+1}$ with $\alpha_{2n+1}\neq 0$ for $n=0$ and 1. It has been shown that the Rayleigh type oscillator presents good stability and a strong attractor [5,6,14–16]. Bifurcations and chaos have been observed theoretically in MAEMS described by equation of the form (3) and (4) [10] and in MaEMS with rigid arm [5,6]. Extension has been made on synchronization of MaEMS [5,6].

Considering all the potentially interesting applications and theoretical work done so far on the dynamics of self-sustained MaEMS, a very important step should be reached, that is the realization and experimental study of such systems. In this paper, we extend the work in [10] to experimental simulation. Analog simulation of a self-sustained mass–spring-damper system described in Refs. [5,6] is shown in Ref. [17] while the experimental realization and simulation is shown in Ref. [13]. A Rayleigh–Duffing (RD) oscillator driving a mechanical flexible arm is considered. In order to increase the actuating mechanical force, the device is modified by integrating an audio amplifier. A brief discussion of the characteristics of the audio amplifier is given. The modeling equations of the device are then derived. Three nonlinear phenomena are investigated: quenching phenomenon, bifurcation and chaos. Finally, a nonlinear MaEMS is designed and fabricated. Experimental verification of the theoretical results is then made. Experimental behavior of the mechanical arm is verified using a motion detector or an accelerometer.

The paper is presented as follows. Section 2 deals with the characterization of the audio amplifier and the modeling equations of the system are derived. Section 3 presents results from theoretical analysis while in Section 4, those from experimental simulations are presented. Section 5 is for the conclusion and hints of applications.

2. The modified EMS

We consider the device of Fig. 1. The device is made up of an electric implementation of a Rayleigh–Duffing oscillator actuating a mechanical cantilever arm. The mechanical arm is a flexible structure, which is connected to the magnet through a thin rigid rod. Between the electric circuit and the permanent magnet, the device is modified by adding an audio amplifier in order to increase the delivery electric signal to the magnet and consequently, the Laplace actuating force. In fact, a simple analysis shows that for such devices, without the amplifier, the Laplace force is in the order of 10^{-2} N for a magnet in the same order, and in order to move the mechanical arm the require force is in the order of 10^{-1} N (the order of the weight of the mechanical elements). Moreover, the natural frequency of the RD oscillator is generally greater than 1 kHz while the natural frequency of the mechanical arm is in the Hz domain. All these frequencies belong to the audio frequency. These problems of amplitude and frequency can be generalized to MaEMS and, contrasted with MEMS and NEMS. As generally done for magnetic bearing systems [1,2,7–9] an amplifier can be used to increase the amplitude of the signal. The amplifier is made of an integrated circuit of type TDA2050 [18] polarized with direct current (DC) of voltage of 50 V; it presents a very low distortion output signal and a higher output power 50 W. The parameters of the audio amplifier are listed in Table 1; with these parameters, the device presents a voltage gain of 27 and it can also affect the output frequency. We use an operational amplifier of type LF352N and multiplier of type AD633 polarized with a DC voltage 12 V.

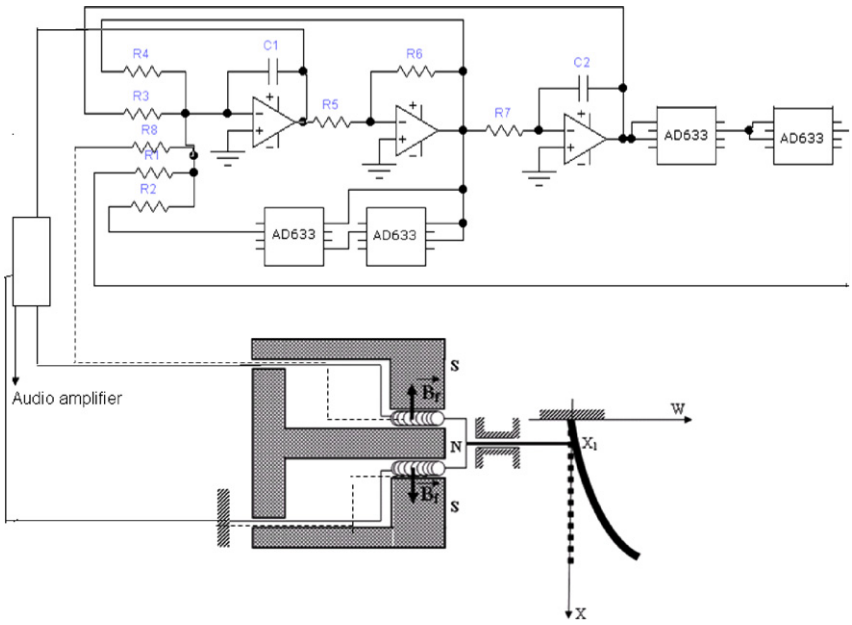

Fig. 1. The modified self-sustained EMS.

Table 1
Parameter of the audio amplifier.

Components	Symbol	Values	Units
Resistance	R_1	22,000	Ω
	R_2	22,000	Ω
	R_3	22,000	Ω
	R_4	10,000	Ω
	R_5	330	Ω
	R_6	10	Ω
Capacitance	C_1	47×10^{-6}	F
	C_2	1×10^{-6}	F
	C_3	3.3×10^{-3}	F
	C_4	47×10^{-6}	F
	C_5	10^{-8}	F
Polarization	V_{cc}	50	V
Input impedance	Z_e	500	kΩ
Output impedance	Z_s	4	Ω

The analog method provides a number of facilities for controlling dimensionless parameters. In fact, it is easier to change a dimensionless parameter by adjusting only one experimental component [17,19]. A second coil is added to the system for a feedback connection of the mechanical part (wire represented by dashed line).

2.1. Characteristic equations of the audio amplifier

Assume a voltage V at the input of the audio amplifier is delivered in the coupling domain (see Fig. 2). After some calculations [20], one obtains the following expressions for the current i_0 through the magnet and the output voltage v_s

$$v_s = A_{12}V - A_{11}Bl_0\frac{\partial y}{\partial t}\delta(x-x_1), \tag{5}$$

$$i_0 = A_{22}V - A_{21}B_f l_0\frac{\partial y}{\partial t}\delta(x-x_1), \tag{6}$$

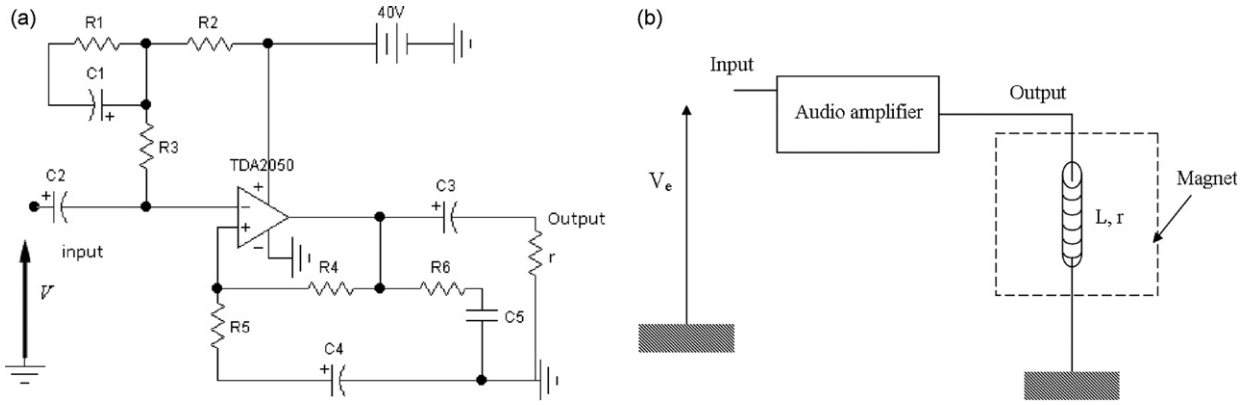

Fig. 2. The audio amplifier: (a) synoptic of the amplifier; (b) synoptic of the coupling.

with

$$A_{11}=\frac{R_0}{\Delta},\quad A_{12}=\frac{\left[r\left(1+\frac{R_4+R_0}{R_2}\right)+R_0\left(1+\frac{R_4}{R_2}\right)\right]}{\Delta},$$

$$A_{21}=\frac{1+\frac{A_vR_0}{Z_s}+\frac{R_0+R_4}{Z_e\oplus R_2}}{\Delta},\quad A_{22}=\frac{1}{\Delta}\left[\frac{R_0}{Z_e}+\frac{A_vR_0}{Z_s}\left(1+\frac{R_4}{R_2}\right)\right],$$

$$\Delta=R_0\left[1+\frac{R_4}{Z_e\oplus R_2}\right]+r\left[1+\frac{A_vR_0}{Z_s}+\frac{R_0R_4}{Z_e\oplus R_2}\right],$$

$$R_0=R_3\oplus Z_s,\quad A_v=\frac{Z_e}{Z_e+Z_s}K_0\exp\left(\frac{V_{cc}}{V_0}\right),\quad K_0=875\quad\text{and}\quad V_0=20\,V, \tag{7}$$

where r is the total resistance of the induced circuit, the symbol $R_i\oplus R_j$ gives the equivalent resistance of R_i and R_j taken in parallel.

All physical parameters of the audio amplifier are fixed. In the rest of the paper, the labels above for the resistances and condensers are used to designate the parameter of the RD oscillator. Without loss of generality, the value L of the self in the coupling domain is neglected.

2.2. Modeling equation of the device

Using Newton and Hooke laws for the mechanical arm and Kirchhoff laws for the electric circuit, the following set of coupled nonlinear differential equations for the device are obtained

$$\frac{d^2v_s}{d\tau^2}-\varepsilon_1\frac{dv_s}{d\tau}\left[1-\left(\frac{dv_s}{d\tau}\right)^2\right]+\omega_0^2v_s+\beta v_s^3=-\frac{n_2B_fl_0\alpha R_5T}{n_1R_8R_6R_7C_1C_2}\frac{\partial W}{\partial\tau}\delta(X-X_1), \tag{8}$$

$$S\rho\frac{\partial^2W}{\partial\tau^2}+\left[\lambda+\frac{B_f^2l_0^2A_{21}}{l}\delta(X-X_1)\right]\frac{\partial W}{\partial\tau}+EI\frac{\partial^4W}{\partial X^4}=\frac{B_fl_0A_{22}R_6R_7C_2}{lR_5\alpha\omega_0}\frac{dv_s}{d\tau}\delta(X-X_1) \tag{9}$$

where W is the transversal displacement taking as a function of time τ and abscisse X (see Fig. 1), v_s is the electric signal delivered by the RD oscillator. S is the transversal section of the flexible arm, ρ the mass density, E the Young modulus, I the moment of inertia, $-\lambda\frac{\partial W}{\partial\tau}$ is the load arising from the viscosity of the air and friction in the coupling domain, l the length of the flexible arm, B_f is the intensity of the magnet, l_0 the length of the copper wire used in the coupling domain, X_1 the contact point on the flexible arm and $\delta(.)$ stands for the Dirac delta function. The physical and geometrical value of the parameters of the flexible arm are given in Table 2. The other parameters of Eqs. (8) and (9) are defined as functions of electric components as follows

$$\varepsilon_1=\frac{R_7Tv}{R_4R_6C_2},\quad v=\frac{R_7C_2}{R_4C_1},\quad \omega_0=\sqrt{\frac{R_5T^2}{R_3R_6R_7C_1C_2}},\quad \beta=\frac{R_5T^2}{100R_1R_6R_7C_1C_2\alpha^2},$$

$$\alpha=\sqrt{\frac{R_7^3C_2^3}{100vR_2C_1T^2}}\quad\text{and}\quad T=10^{-5}\quad\text{is a characteristic time constant [1].}$$

Table 2
Characterization of the mechanical arm.

Designation	Symbol	Values	Units
Mass density	ρ	1.60	$10^3\,\mathrm{kg\,m^{-3}}$
Young modulus	E	6.10	$10^{11}\,\mathrm{N\,m^{-2}}$
Length	l	205	mm
Thickness	h_0	0.5	mm
Width	h_1	21	mm
Natural frequency	$\frac{k^2}{l^2}\sqrt{\frac{EI}{h_0h_1\rho}}$	48.3	Hz

The boundary conditions are given as

$$W(X,\tau)=\frac{\partial W(X,\tau)}{\partial X}=0 \quad \text{at} \quad X=0 \quad \text{and}$$
$$\frac{\partial^2 W(X,\tau)}{\partial X^2}=\frac{\partial^3 W(X,\tau)}{\partial X^3}=0 \quad \text{at} \quad X=l \tag{10}$$

the boundary conditions express that the displacement and rotation are constraned to zero at $X=0$ and the shear force and bending moment are constrained to zero at $X=l$.

In dimensionless form, Eqs. (8) and (9) are rewritten as

$$\frac{\mathrm{d}^2u_s}{\mathrm{d}t^2}-\varepsilon_1\frac{\mathrm{d}u_s}{\mathrm{d}t}\left[1-\left(\frac{\mathrm{d}u_s}{\mathrm{d}t}\right)^2\right]+\omega_0^2u_s+\beta u_s^3=-\eta_0\frac{\mathrm{d}y}{\mathrm{d}t}\delta(x-x_1), \tag{11}$$

$$\frac{\partial^2 y}{\partial t^2}+\varepsilon_2\frac{\partial y}{\partial t}+a_1^2\frac{\partial^4 y}{\partial x^4}=\eta_2\frac{\mathrm{d}u_s}{\mathrm{d}t}\delta(x-x_1), \tag{12}$$

with

$$y(x,t)=\frac{\partial y(x,t)}{\partial x}=0 \quad \text{at} \quad x=0 \quad \text{and}$$
$$\frac{\partial^2 y(x,t)}{\partial x^2}=\frac{\partial^3 y(x,t)}{\partial x^3}=0 \quad \text{at} \quad x=l \tag{13}$$

and

$$\varepsilon_2=\frac{\lambda T}{\rho S}+\frac{A_{21}B_f^2l_0^2T}{\rho S}\delta^2(x-x_1), \quad a_1=\sqrt{\frac{EIT^2}{\rho Sl^4}}, \quad \eta_2=\frac{B_fl_0A_{22}TR_6R_7C_2U}{l^2R_5\alpha\rho S}, \quad \eta_0=\frac{B_fl\alpha A_{21}rR_5\omega_0^2l_0}{R_8R_6R_7C_1C_2U},$$

where v_s has been normalized relative to a characteristic voltage of $U=1\,\mathrm{V}$, $y=W/l$, and $t=T\tau$.

3. Nonlinear phenomena in the modified EMS

Many works have been devoted to mathematical analysis and numerical simulation of a device modeled by equations of the type (8) and (9), see Refs. [1–10] for instance. Amongst useful nonlinear phenomena found, there are quenching phenomenon, bifurcation, chaos, sub and super harmonic, and hysteresis. In the following section, our attention is focused on quenching phenomenon, bifurcation and chaos. In fact, many engineering applications can be found for these phenomena as discussed later on in this paper.

3.1. Quenching phenomenon

For a set of parameters of a MaEMS, the device can remain at rest (at the stable static equilibrium) even if one or two parts of the device taken alone are in a dynamical state. This is the so-called quenching phenomena. Quenching phenomena was earlier reported in self-sustained dynamics by Tondl [16] in 1976. From linear stability analysis [15], one can show that the unique fixed point $(u_s=0, \mathrm{d}u_s/\mathrm{d}t=0, y=0, \partial y/\partial t=0)$ of Eqs. (11) and (12) is stable for

$$\varepsilon_1<\varepsilon_2, \tag{14}$$

$$\varepsilon_2-\frac{\eta_{0m}\eta_{2m}}{\varepsilon_1}<-\frac{\varepsilon_2(\hat{\alpha}_0^2-1)^2\omega_0^2}{(\varepsilon_2-\varepsilon_1)(\varepsilon_2-\varepsilon_1\hat{\alpha}_0)}\le 0 \tag{15}$$

with

$$\eta_{im}=\eta_i\frac{\sin kx_1+\sinh kx_1}{\cos kx_1+\cosh kx_1}[\cosh kx_1-\cos kx_1]+\sin kx_1-\sinh kx_1,\quad i=0;$$
$$2\cos k\cosh k+1=0,\quad \alpha_0=\frac{\omega_0}{\omega_{0m}},\quad \text{and}\quad \omega_{0m}=a_1^2k,. \tag{16}$$

The expression of η_{im} is obtained after transforming Eqs. (8) and (9) into a set of two ordinary differential equations using the Galerkin modal approximation limited to a single mode of vibration. The subscript m stands for the mode of vibration. The reader is invited to see Ref. [10] for details. The linear stability of the unique steady state of the system induces the mathematical conditions for the quenching phenomenon. In fact if conditions (14) and (15) are satisfied, there will be no mechanical response from the system. Inequality (15) can be rewritten as

$$\eta_{0m}>\sup\left[\frac{\varepsilon_2\varepsilon_1}{\eta_{2m}},\frac{\varepsilon_1\varepsilon_2(\tilde{\alpha}_0^2-1)^2\omega_0^2}{\eta_{2m}(\varepsilon_2-\varepsilon_1)(\varepsilon_2-\varepsilon_1\tilde{\alpha}_0)}\right]. \tag{17}$$

This constraint on η_{0m} yields the following constraint for the coupling resistance R_8

$$R_8<\mathrm{Inf}\left[\frac{B_f l\alpha A_{21} r R_5\omega_0^2 l_0}{R_8R_6R_7C_1C_2U}\frac{\eta_{2m}}{\varepsilon_2\varepsilon_1},\frac{B_f l\alpha A_{21} r R_5\omega_0^2 l_0}{R_8R_6R_7C_1C_2U}\frac{\eta_{2m}(\varepsilon_2-\varepsilon_1)(\varepsilon_2-\varepsilon_1\tilde{\alpha}_0)}{\varepsilon_1\varepsilon_2(\tilde{\alpha}_0^2-1)^2\omega_0^2}\right]. \tag{18}$$

Fig. 3 illustrates the quenching phenomenon for the following values of the dimensionless parameter $\beta=0.01;\varepsilon_1=0.01;$ $\eta_0=0.05$ and $\eta_2=0.2$ which correspond to the physical values listed in Table 3a (a refers to the third column of the table) with the frequency of the electric circuit equal to 141 kHz, while the mechanical one is 48.3 Hz. These curves present the

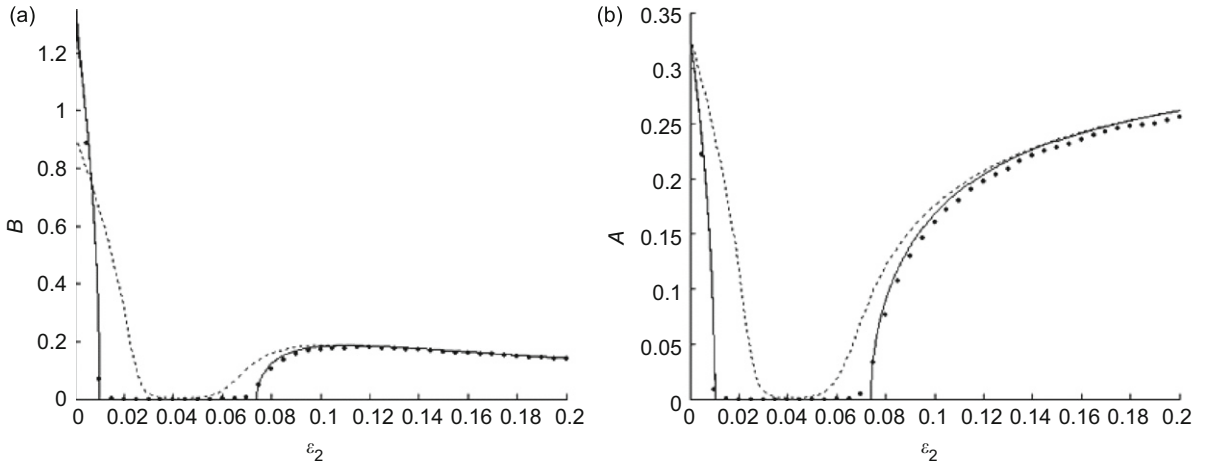

Fig. 3. Theoretical illustration of the quenching phenomenon: (a) amplitude of the electrical part; (b) amplitude of the mechanical part.

Table 3
Physical values of the parameters of the RD oscillator for quenching phenomena.

Components	Symbol	Theoretical values	Experimental values	Units
Resistance	R_1	11.9	11.9	Ω
	R_2	178	178	Ω
	R_3	98	98	Ω
	R_4	5000	4680	Ω
	R_5	23 426	9850	Ω
	R_6	9860	9860	Ω
	R_7	3320	3320	Ω
	R_8	Variable	Variable	Ω
Capacitance	C_1	4.47×10^{-8}	12.68×10^{-9}	F
	C_2	1.6×10^{-8}	12.18×10^{-9}	F
Magnet	B_f	16	16	mT
Length of wire	l_0	54	54	m
Resistance of the coupling zone	r	4	4	Ω

maximum amplitude of the electric signal and mechanical displacement (at the free end) as a function of the mechanical dissipative coefficient ε_2. For $0.035 < \varepsilon_2 < 0.06$, the amplitude response of the two parts of the system is zero. The results are obtained from finite difference simulation of Eqs. (11) and (12) (curve in dashed line), Galerkin approximation (curve in point) and averaging method (curve in line). See Ref. [14] for details on the calculations and simulations. This double inequality of ε_2 suggest the domain of the overall damping coefficient for the quenching phenomenon, that is $\lambda \in]0.664; 1.189[$ in kgs^{-1}.

3.2. Bifurcation and chaos

Many chaotic indicators are generally used to find chaos in dynamical system [3–6,10]. Amongst them, the Lyapunov exponent is the most precise. The Lyapunov exponent expresses the convergence (when negative) or the divergence (when positive) of nearby trajectories. Therefore, a system is said to be chaotic if the exponent is positive which corresponds, in the bifurcation diagram, to a cloud of points. The system is said to be periodic if the exponent is negative, this corresponds to a curve lines in the bifurcation diagram. The exponent is computed as

$$\mathrm{lyn} = \lim_{t\to\infty} \frac{\ln(d(t))}{t} \quad \text{with } d = \sqrt{\delta q^2 + \left(\frac{\mathrm{d}\delta q}{\mathrm{d}t}\right)^2 + \sum_{i=1}^{n} \delta v_i^2 + \sum_{i=1}^{n} \left(\frac{\partial \delta v_i}{\partial t}\right)^2}, \tag{19}$$

where δq and δv_i are respectively the variations of q and v_i. In this expression, $v_i = v(ih,t)$, $h = 1/n$ and n being the number of the discrete infinitesimally interval considered on the flexible arm length. Fig. 4a presents the exponent as a

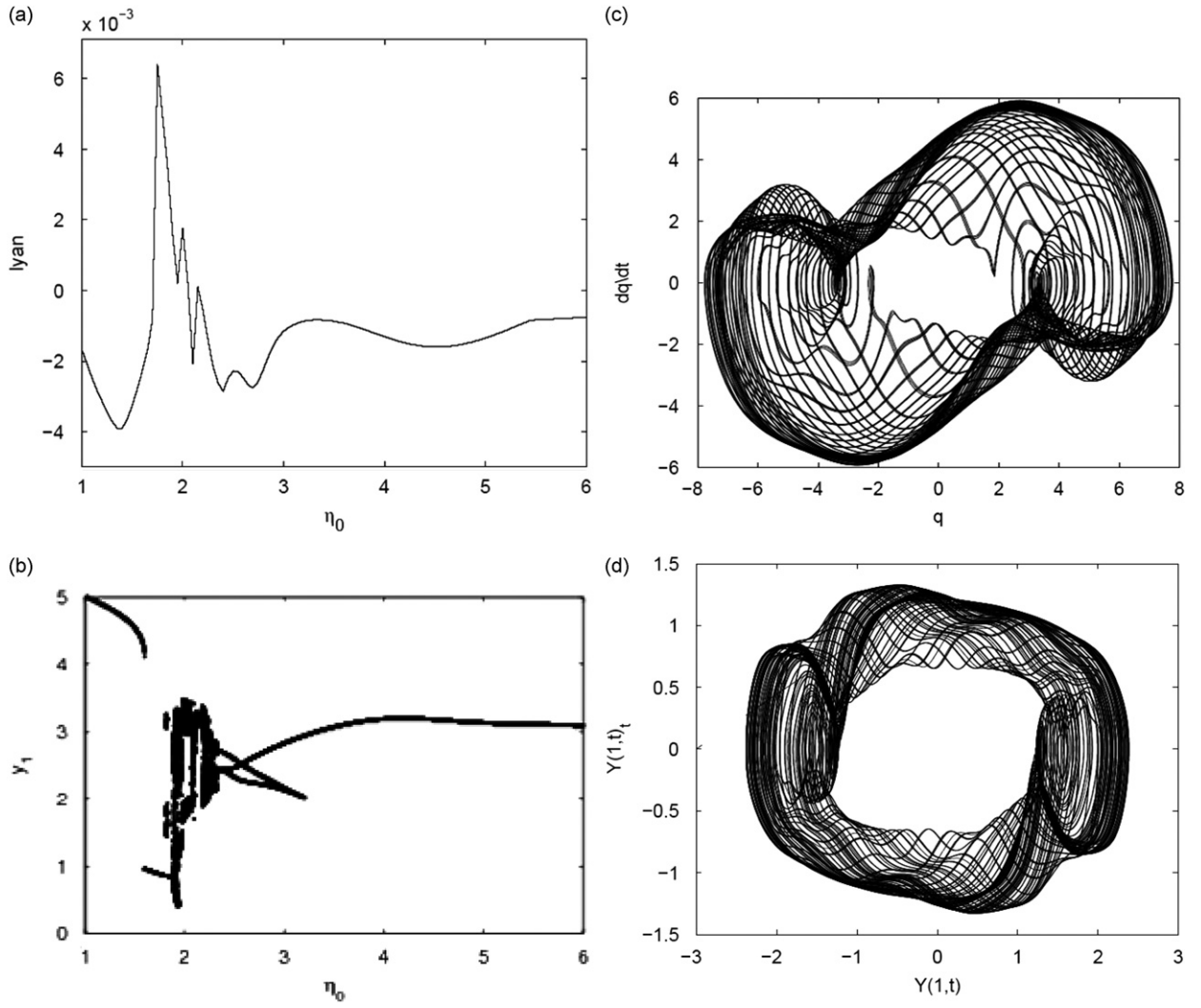

Fig. 4. Chaotic characterization of the device: (a) Lyapunov exponent; (b) bifurcation diagram of the mechanical arm; (c) chaotic phase diagram of the electric part; (d) chaotic phase diagram of the mechanical part.

Table 4
Physical values of the parameters of the RD oscillator for bifurcation and chaos.

Components	Symbol	Theoretical values	Experimental values	Units
Resistance	R_1	11.9	11.9	Ω
	R_2	178	178	Ω
	R_3	98	98	Ω
	R_4	5000	4680	Ω
	R_5	97.3	9850	Ω
	R_6	9860	9860	Ω
	R_7	3320	3320	Ω
	R_8	Variable	Variable	Ω
Capacitance	C_1	1.8×10^{-8}	1.6×10^{-6}	F
	C_2	1.6×10^{-8}	3.3×10^{-6}	F
Magnet	B_f	16	16	mT
Length of wire	l_0	54	54	m
Resistance of the coupling electment	r	4	4	Ω

function of the coupling coefficient η_0 for a set of system parameters defined as $\beta=0.01$, $\varepsilon_1=2.466$, $\eta_2=3.518$, $\sigma=0$, $\varepsilon_2=0.01$ which correspond to the physical values of Table 4. The corresponding bifurcation diagram of the mechanical arm is shown in Fig. 4b. One finds from these curves that, for $\eta_0\in[1.85;2.3]$, there is a series of domains corresponding to chaotic dynamics, out of this domain, the device has a periodic motion. The chaotic phase portrait of the system plotted in Fig. 4c (for the electric part) and Fig. 4d (for the mechanical part), for a value of $\eta_0=2.2$ using finite difference simulation, is consistent with the bifurcation diagram and the Lyapunov exponent.

4. Experimental verification of nonlinear phenomena

4.1. The readout principle

The best way to measure the dynamical characteristic of an oscillating body is to use either a motion detector or an accelerometer. Here an accelerometer of type DE-ACCM2G polarized with a DC voltage of 3.5 V is used. The accelerometer is attached on the mechanical arm and the delivered electric signals are observed through an oscilloscope of type HM303-6 (Hameg Instrument). The device delivers a good signal only for high frequencies (>100 kHz); for a low frequency, the signals delivered have been found to be very weak and have appeared as noise on the oscilloscope. Thus, for lower frequencies the video analyzer function of a motion detector of type Looger Pro 3.6.1 is used. Data are extracted from the video of the displacement of the mechanical arm. To observe the signal from the electronic circuit, a two-input probes oscilloscope is used. The inputs are then connected to the points corresponding to the founding target signal on the electric circuit.

An experimental model of nonlinear MaEMS, shown in Fig. 1, has been designed and fabricated. A photographic image of the parts of the device is shown in Fig. 5. In the experiment, the frequency of the electric circuit differs slightly from that of the mechanical part; moreover, according to Sections 2 and 3, imperfections in the fabricated structure will affect quantitatively our results. However, since R_8 affects only the coupling term η_0, the device can still be turned to give more accurately or complex behaviors for another set of values of the parameters of the MaEMS.

4.2. Quenching phenomenon

In order to test whether the device can experimentally achieve quenching phenomenon, we have taken the values of Table 3b (b stands for the fourth column of the table) which correspond to $\beta=0.04;\varepsilon_1=0.042;\eta_2=7.5\times10^{-8}$ and $\eta_0=1.3\times10^{12}/R_8$. We observed that as the RD device oscillates, if we connect the mechanical arm, both parts of the system become at rest. For instance, after connecting the flexible arm and increasing the coupling resistance R_8 from $0\,\Omega$, both parts of the system do no longer vibrate. The phenomenon can be explained as a result of quenching phenomenon in both parts of the system. That is, the connection of the flexible arm annihilate the oscillations. The interval of quenching phenomenon is obtained using relation (15) (that is the interval of the stability of trivial fixed point). It is observed that the quenching phenomenon appears for all $R_8<2.8\times10^6\Omega$. The quenching phenomenon is illustrated experimentally by whistling on the coupling domain and by noise (signal with very low amplitude and poor quality) on the oscilloscope.

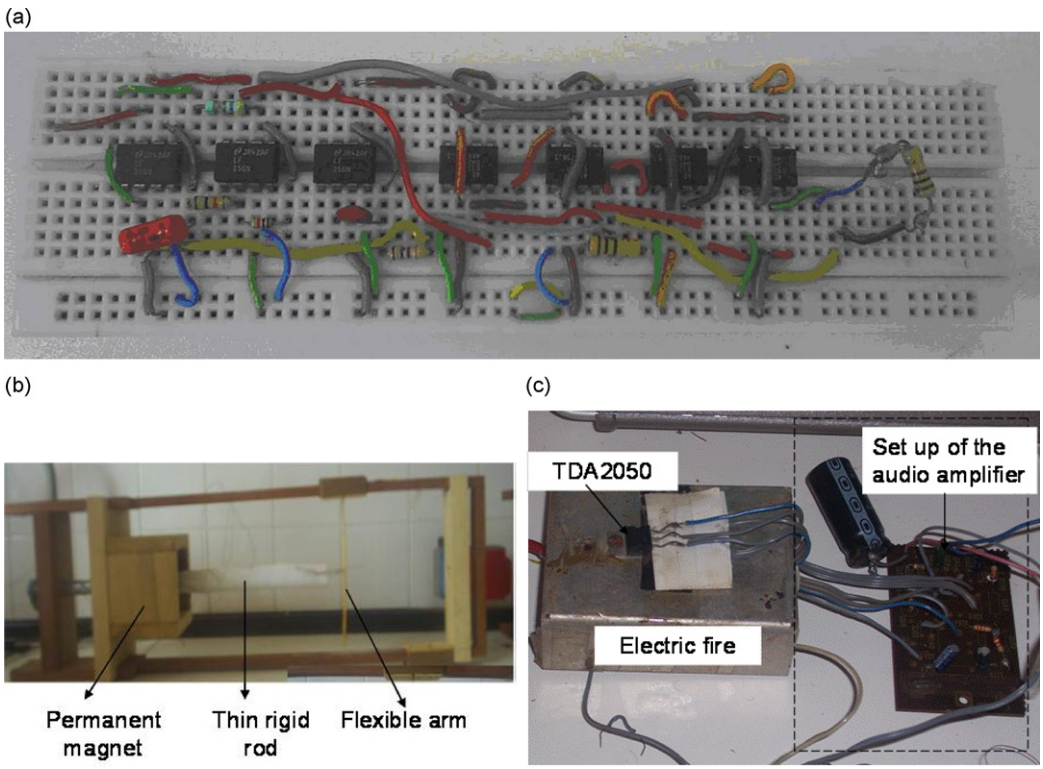

Fig. 5. Experimental realization of the device: (a) the electric circuit; (b) the mechanical arm; (c) the audio amplifier.

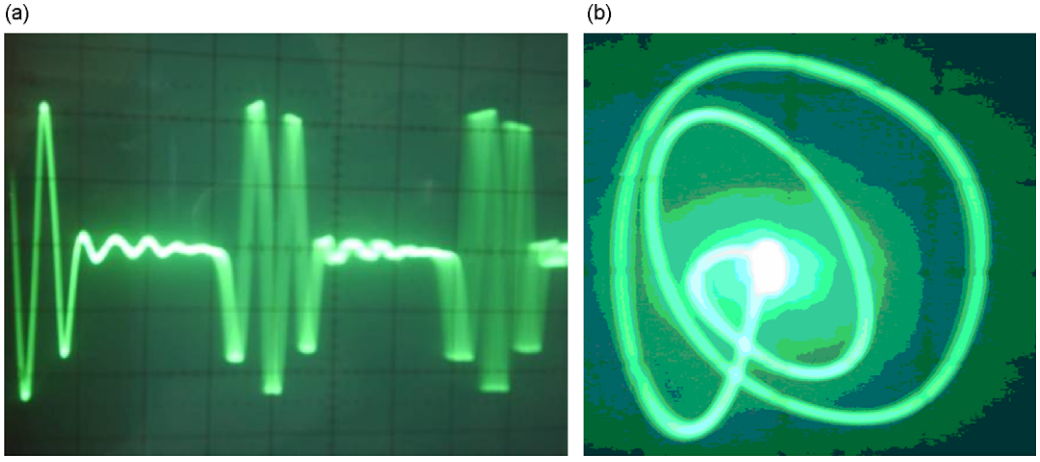

Fig. 6. Periodic behavior of the electric circuit: (a) temporal evolution; (b) phase portrait.

4.3. Bifurcation and chaos

Regarding bifurcations and chaos in the system, we change two parameters of the RD oscillator according to $C_1 = 1.5 \times 10^{-6}\,\mathrm{F}$ and $C_2 = 3.3 \times 10^{-6}\,\mathrm{F}$, which corresponds to a frequency of 787.58 Hz (low frequency) and $\beta = 1.6 \times 10^{-11}; \varepsilon_1 = 3.5 \times 10^{-4}; \eta_0 = (3.4 \times 10^5)/R_8$ and $\eta_2 = 7.5 \times 10^{-8}$. By varying R_8, a sequence of bifurcations with regular and chaotic dynamics is obtained. Regular dynamics is obtained for $R_8 < 2.2\,\mathrm{k\Omega}$. For $R_8 = 1\,\mathrm{k\Omega}$ ($\eta_0 = 3.4 \times 10^5$), temporal evolution and phase portraits in $(v_s, \mathrm{d}v_s/\mathrm{d}t)$ and $(y(1,t), \partial y/\partial t(1,t))$ planes are plotted in Figs. 6 and 7. Fig. 6 is a photographic image of the oscilloscope and Fig. 7 is obtained from a motion detector. The curves illustrate multiperiodic dynamics with "breathing". The "breathing" is caused by the elasticity of the mechanical arm. For the electric signal, the scale is 2 V per division and the maximum voltage is obtained as 4 V. The two maxima are approximatively equals. For the mechanical part, a direct measurement gives for the deflection 1.6 and 1.3 cm.

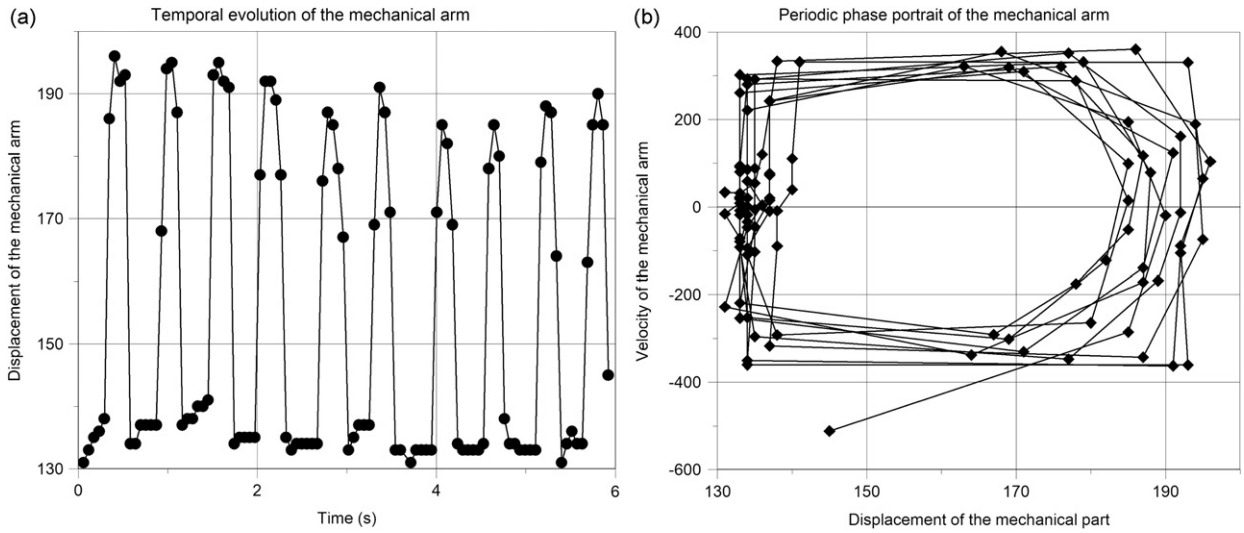

Fig. 7. Periodic behavior of the mechanical arm: (a) temporal evolution; (b) phase portrait.

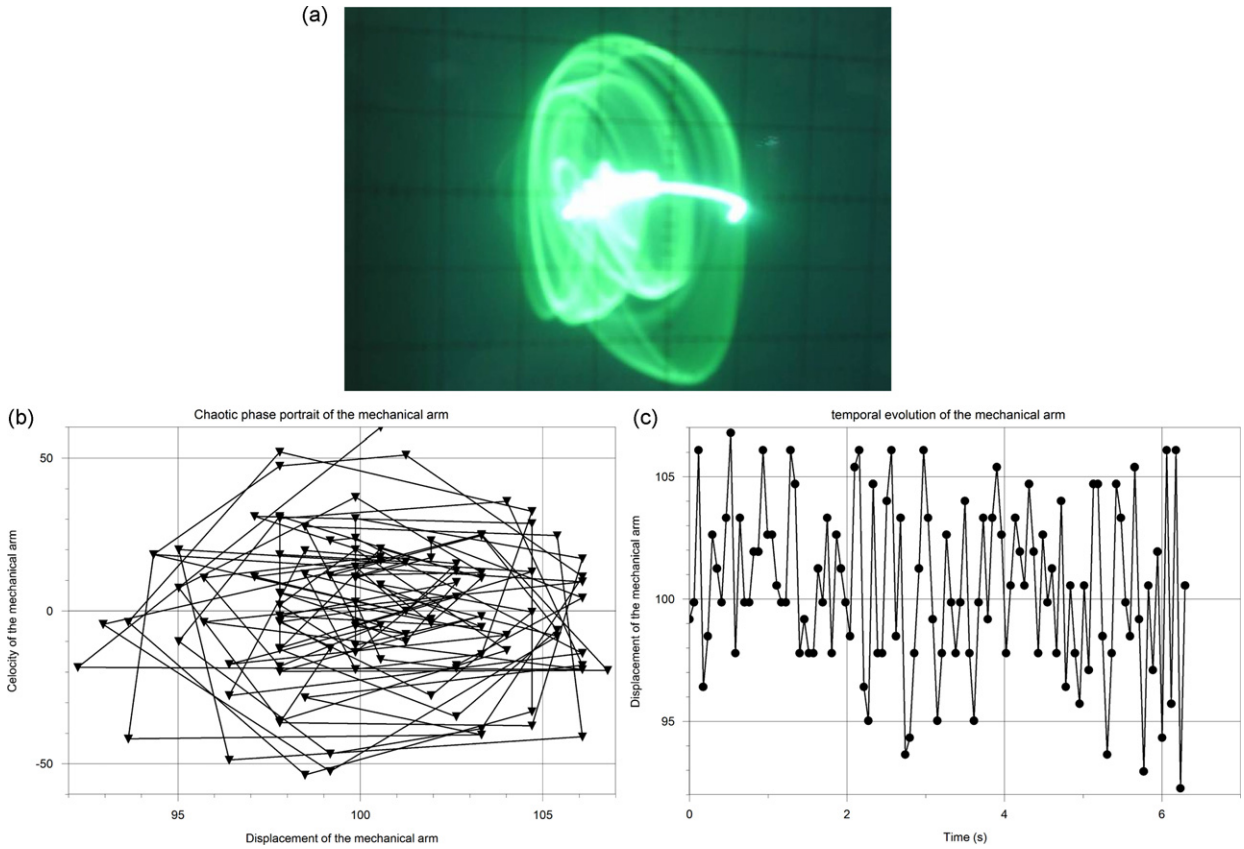

Fig. 8. Chaotic phase portrait: (a) the electric circuit; (b) the mechanical arm; (c) the temporal evolution of the mechanical arm.

Chaotic behavior is illustrated by the phase portrait plotted in Fig. 8 for $R_8 = 2.6\,\mathrm{k\Omega}$ ($\eta_0 = 130.77$). The system remains in a chaotic behavior until a larger value of R_8 where the quenching phenomenon appears. This bifurcation sequence qualitatively agrees with the bifurcation diagram plotted in Fig. 4b.

A remark here is that, although, we have assumed that there is a signal going from the amplifier to the electronic circuit (by idealizing the composites), the effect of the audio amplifier can be observed experimentally as a weak signal. This can

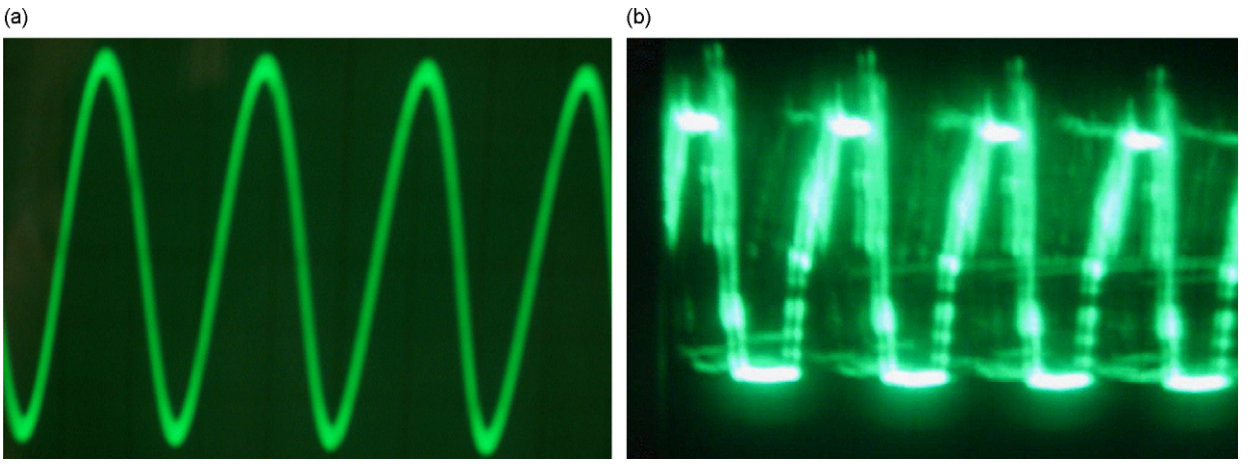

Fig. 9. Acceleration of the mechanical arm for higher frequency: (a) for $\omega = 100$ kHz; (b) for $\omega = 10$ kHz.

be the cause of a slight difference between theoretical and experimental results. Another remark is that as the audio amplifier affects the electric output frequency, despite the device is far from resonance, there is a mechanical motion.

To see experimentally what happens at a higher frequency, we set $R_7 = 1\,\text{k}\Omega$ and $R_8 = 100\,\text{k}\Omega$ and vary C_2 from 10 nF to 0.25 mF, that is to vary the frequency of the electric signal from 150 to 1 kHz. The other parameters are defined as above. As the control parameter varies, the acceleration of the mechanical arm is quite clear for higher frequencies 150 kHz for C_2=10.72 nF (Fig. 9a) and becomes a sort of noisy dressing and asymmetrical shape for C_2=2.4 nF corresponding to 10 kHz (Fig. 9b). It is quite difficult to determine the value of the deflection since the displacement is very weak. Thus, very far from resonance, even with the audio amplifier, the mechanical arm is near the steady state. These results have been obtained theoretically [5–7] and experimentally [13] in MaMES.

5. Conclusion

In this paper, a self-sustained MaEMS was considered. The device is made up of an electric implementation of a RD oscillator driving a flexible arm. The RD was designed using analog components. An audio amplifier has been integrated in order to avoid experimental constraints. Using linear stability analysis, the Lyapunov exponent and bifurcation diagram, quenching phenomenon and chaos have been predicted to occur in the behaviors of the device. An experimental model was fabricated and by tuning the coupling resistance, experimental results agree with the theoretical ones. A slight difference in some physical values is observed due to imperfections in the experimental model and various approximations.

Results of the work are relevant to a broad variety of applications including actuation, mixing, energy autonomy and switches. The device presents bifurcations and chaotic behavior which can be used in the optimization process such as shaking, mixing and manufacturing chain. The quenching phenomenon can be used in switching conditions to avoid oscillation corresponding to a given value of the system parameter.

Acknowledgments

This work is supported by the Academy of Science for developing World—TWAS under Research Grant No. 03-322 RG/PHY/AF/AC.

C.A. Kitio Kwuimy would like to thank the African Institute of Mathematical Science—AIMS, for the facilities.

References

[1] A. Preumont, *Mechatronics: Dynamics of Electromechanical and Piezoelectric Systems*, Springer, Dordrecht, 2006.
[2] J. Jerrelind, A. Stensson, Nonlinear dynamics of parts in engineering systems, *Chaos, Solitons and Fractals* 11 (2000) 2413–2428.
[3] A.C.J. Luo, F. Wang, Chaotic motion in a microelectromechanical system with non-linearity from capacitors, *Communications in Nonlinear Science and Numerical Simulation* 7 (2002) 31–49.
[4] B. DeMartini, H. Butterfield, J. Moehlis, K. Turner, Chaos for a microelectromechanical oscillator governed by the nonlinear Mathieu equation, *Journal of Microelectromechanical Systems* 16 (2007) 1314–1323.
[5] J.C. Chedjou, P. Woafo, S. Domngang, Shilnikov chaos and dynamics of a self-sustained electromechanical transducer, *Journal of Vibration and Acoustics* 123 (2001) 170–174.
[6] R. Yamapi, P. Woafo, *Nonlinear Electromechanical Devices: Dynamics and Synchronisation, Mechanical Vibrations: Measurement, Effects and Control*, Nova Science Publishers, 2005.

[7] J.C. Ji, Stability and Hopf bifurcation in a magnetic bearing system with time delays, *Journal of Sound and Vibration* 259 (2002) 845–856.
[8] J.C. Ji, Stability and bifurcation in an electromechanical system with time delay, *Mechanics Research Communications* 30 (2003) 217–225.
[9] J.C. Ji, C.H. hansen, A.C. Zander, Nonlinear dynamics of magnetic bearing systems, *Journal of Intelligent Material System and Structures* 12 (2008) 1471–1491.
[10] C.A. Kitio Kwuimy, P. Woafo, Dynamics, chaos and synchronization of self-sustained electromechanical systems with clamped-free flexible arm, *Nonlinear Dynamics* 53 (2008) 201–214.
[11] J.L. Palacios Felix, J.M. Balthazar, Comments on a nonlinear and nonideal electromechanical damping vibration absorber, Sommerfeld effect and energy transfer, *Nonlinear Dynamics* 53 (2009) 111.
[12] J.L. Palacios Felix, J.M. Balthazar, R.M.L.R.F. Brasil, Comments on nonlinear dynamics of a non-ideal Duffing–Rayleigh oscillator: numerical and analytical approaches, *Journal of Sound and Vibration* 319 (2009) 1136–1149.
[13] C.A. Kitio Kwuimy, P. Woafo, Experimental realization and simulations a self-sustained macro electromechanical system, *Mechanics Research Communications* 37 (2010) 106–110.
[14] R.H. Rand, *Lectures Notes on Nonlinear Vibrations*, Cornell University, New York, 2005.
[15] C. Hayashi, *Nonlinear Oscillations in Physical Systems*, Mc Graw-Hill, New York, 1964.
[16] A. Tondl, Quenching of self-excited vibrations. Effect of dry friction, *Journal of Sound and Vibration* 45 (2) (1976) 285–294.
[17] J.C. Chedjou, H.B. Fotsin, P. Woafo, S. Domngang, Analog simulation of the dynamics of a van der pol oscillator coupled to Duffing oscillator, *IEEE Transaction on Circuit and System—Fundamental Theory and Applications* 748 (2001) 48–58.
[18] 〈http//www.datasheetarchive.com〉.
[19] A. Ismael Heisler, T. Braun, Z. Ying, H. Gang, A. Hilda Cerdeira, Experimental investigation of partial synchronization in coupled chaotic oscillators, *Chaos* 13 (2003) 185–194.
[20] M. Tooley, *Electronic Circuits: Fundamentals and Applications*, third ed., Elsevier, Oxford, 2006.